P21

Study on Carrier Mobility in Graphene Nanoribbons

Xinxin Yu, Jinyu Zhang*, Jiahao Kang, He Qian, and Zhiping Yu
Institute of Microelectronics,
Tsinghua University
Beijing, China 100084
zhangjinyu@tsinghua.edu.cn

Yaohua Tan
Network for Computational Nanotechnology
Purdue University,
West Lafayette, IN 47907, USA

***Abstract*—In this paper, the carrier mobility in graphene nanoribbons(GNRs) is studied. The total carrier mobility calculation includes four scattering mechanisms: surface polar phonons (SPP) scattering, intrinsic acoustic phonon scattering, line-edge roughness scattering, and Coulomb scattering. Carrier SPP scattering rates for five high-κ dielectric materials, including SiO_2, Al_2O_3, HfO_2, ZrO_2 and AlN, are calculated based on Mahan's theory. SPP scattering turns out to be important for GNRs with small width. Compared to other dielectric materials, AlN is more capable of suppressing both SPP scattering and Coulomb scattering.**

Keywords-graphene nanoribbon; mobility; surface polar phonon

I. Introduction

Graphene with a high mobility of 2×10^5 $cm^2/(V\cdot s)$ [1] has drawn great research interest, especially in recent years. The success in fabricating sub-10 nm width graphene nanoribbon (GNR) field-effect transistors (FETs) [2] shows that GNRs are a promising material for next-generation microelectronic devices channel materials and interconnect. This, however, leads to decrease in carrier mobility, which should also be greatly considered. High-κ dielectric materials, which are extensively used as gate dielectrics to enhance the ability to control the gate, can have a large influence on channel carrier mobility [3]. Due to the polar nature and soft bond of high-κ dielectrics, the carriers in a channel are easy to couple with phonons at the dielectric interface created by the long-range polarization field in high-κ dielectric materials. Several research works have been conducted on the influence of gate dielectrics on carrier mobility in graphene [4][5]. Theoretical calculations of carbon nanotube (CNT) mobility reflect that surface polar phonons (SPP) scattering originating from the dielectric can be quite strong for polar substrates for small diameter CNTs [6]. To the best of our knowledge, SPP scattering in GNR has not been addressed up to now. In this work, the gate dielectric influences are studied by exploring the coupling between the SPP of different dielectrics and the electrons in GNRs. Moreover, four scattering mechanisms, including acoustic phonon (AP) scattering, optical phonon scattering, screened Coulomb scattering, line-edge roughness (LER) scattering, are compared to understand their effects on total carrier mobility.

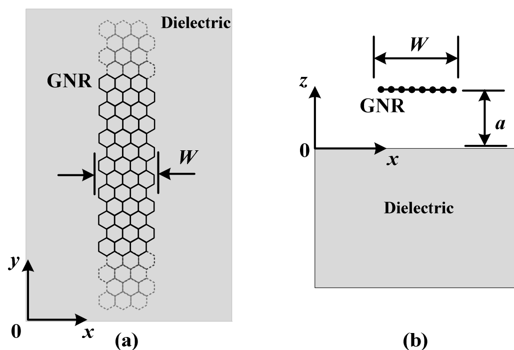

Figure 1. Schematic representation of the GNRs and SPP that cause scattering of mobile carriers: (a) top view and (b) cross section.

II. Theoretical model

A. SPP scattering

In our work, two transverse optical phonon modes exhibiting the largest oscillator strength are considered for five dielectrics. In bulk dielectrics, the frequency dependence of the dielectric constant can be written as [3]

$$\varepsilon_{ox}(\omega)=\varepsilon_{ox}^{\infty}+\frac{\varepsilon_{ox}^{i}-\varepsilon_{ox}^{\infty}}{1-\omega^2/\omega_{TO2}^2}+\frac{\varepsilon_{ox}^{0}-\varepsilon_{ox}^{i}}{1-\omega^2/\omega_{TO1}^2} \tag{1}$$

where the subscript ox is for a general dielectric; ε_{ox}^0 and ε_{ox}^∞ are low- and high-frequency permittivity of the dielectric,

Table I. Surface polar phonon modes for different dielectrics. Parameters have been taken from [3].

Quantity(units)	Dielectrics				
	SiO_2	Al_2O_3	AlN	ZrO_2	HfO_2
ε_{ox}^0	3.90	12.53	9.14	24.0	22.00
ε_{ox}^i	3.05	7.27	7.35	7.75	6.58
ε_{ox}^∞	2.50	3.20	4.80	4.00	5.03
$\hbar\omega_{s1}(meV)$	61.0	56.1	83.8	27.2	21.3
$\hbar\omega_{s2}(meV)$	149.0	110.1	113.8	79.2	55.1

978-1-61284-418-3/11/$26.00 © 2011 IEEE

respectively; ω_{TO1} and ω_{TO2} are the angular frequencies of two transverse optical phonon modes; and ε_{ox}^{i} is an intermediate permittivity describing the dielectric response at some intermediate frequency ω_{int}, such that $\omega_{TO1} \leq \omega_{int} \leq \omega_{TO2}$.

Neglecting the dielectric response of the thin GNR layer and assuming a semi-infinite dielectric shown in Fig.1, the frequencies of the corresponding surface modes are determined by the equation $\varepsilon_{ox}(\omega) + 1 = 0$, where "1" in the equation is the dielectric constant for vacuum, which indicates that we are examining the surface polar phonons at the interface between dielectric and vacuum.

The scattering potential of the ith phonon for mode $\boldsymbol{q}$ at position $\boldsymbol{r}=(x,y,a)$ on the GNR surface can be calculated as

$$
\begin{aligned}
V_{i,\boldsymbol{q}}(x,y,a) &= \int_{\Omega} d\boldsymbol{R} \frac{e_0(\boldsymbol{r}-\boldsymbol{R})\cdot \boldsymbol{P}_{\boldsymbol{q}}(\boldsymbol{R})}{|\boldsymbol{r}-\boldsymbol{R}|^3} \\
&= e_0 F_i |\boldsymbol{q}|^{1/2} \int_{-\infty}^{0} dz_R \int_{-\infty}^{\infty} dx_R \int_{-\infty}^{\infty} dy_R \\
&\times \frac{(\boldsymbol{r}-\boldsymbol{R})\cdot\left(\frac{\boldsymbol{q}}{|\boldsymbol{q}|} - i\hat{z}\right) e^{|\boldsymbol{q}|z_R + i\boldsymbol{q}\cdot\boldsymbol{R}}}{|\boldsymbol{r}-\boldsymbol{R}|^3} \\
&= \frac{i2\pi e_0 F_i}{|\boldsymbol{q}|^{1/2}} e^{-|\boldsymbol{q}|a} e^{iq_y y} e^{iq_x x}; i = 1,2
\end{aligned}
\tag{2}
$$

where $\boldsymbol{P_q}(\boldsymbol{R})$ is the polarization field for mode $\boldsymbol{q}$ at spatial position $\boldsymbol{R}$, a is the distance between GNR, F_i is treated as the interaction term to calculate the electron-SO phonon scattering rates[7], Ω denotes the semi-infinite dielectric and e_0 is the electron charge. The above potential is then transformed into $\boldsymbol{k}$-space to obtain the interaction matrix elements as

$$
\begin{aligned}
V_{i,\boldsymbol{kk}',\boldsymbol{q}} &= \langle \varphi_{n'}(\boldsymbol{k}',\boldsymbol{r}) | V_{i,\boldsymbol{q}} | \varphi_n(\boldsymbol{k},\boldsymbol{r}) \rangle \\
&= \int_A d\boldsymbol{r} \varphi_{n'}^*(\boldsymbol{k}',\boldsymbol{r}) V_{i,\boldsymbol{q}}(x,y,a) \varphi_n(\boldsymbol{k},\boldsymbol{r}) \\
&= \frac{\left(1+e^{i(\theta_n-\theta_{n'})}\right)}{4W} \frac{2\pi e_0 i F_i e^{-|\boldsymbol{q}|a}}{|\boldsymbol{q}|^{1/2}} \delta_{k_y^{'}-k_y,q_y} \times T_{n'n}
\end{aligned}
\tag{3}
$$

where $\varphi_n(\boldsymbol{k},\boldsymbol{r})$ is the wave function of armchair GNR [4][8]

$$
\begin{aligned}
\varphi_n(\boldsymbol{k},\boldsymbol{r}) &= \sqrt{\frac{1}{4S}} e^{ik_y y} e^{i(\Delta K/2 - k_n)x} \begin{bmatrix} 1 \\ -e^{i\theta_n} \end{bmatrix} \\
&- \sqrt{\frac{1}{4S}} e^{ik_y y} e^{-i(\Delta K/2 - k_n)x} \begin{bmatrix} 1 \\ -e^{i\theta_n} \end{bmatrix}
\end{aligned}
\tag{4}
$$

where S represents the surface area of GNR, and n and n' are the quantum numbers of the initial and final states, respectively. When $n \neq n'$, it represents the inter-band scattering, whereas, when $n = n'$, it represents the intra-band scattering. $\boldsymbol{k}=(k_n, k_y)$ is wave number in the $\boldsymbol{k}$-space, where k_n represents the quantum-allowed transverse wave number for semiconducting armchair GNR with discrete values depending on the width W; that is, $k_n = \pm n\pi/3W$, with $n = \pm1, \pm2, \pm4, \pm5, \ldots$. $\theta_n = \text{atan}(k_y / k_n)$. $T_{n'n}$ is an integration defined as follows:

$$
\begin{aligned}
T_{n'n} &= \int_0^W dx \left(e^{-i(\Delta K/2 - k_{n'})x} - e^{i(\Delta K/2 - k_{n'})x} \right) \\
&\times \left(e^{i(\Delta K/2 - k_n)x} - e^{-i(\Delta K/2 - k_n)x} \right) e^{iq_x x} \\
&= -i \left[\frac{1}{c_1} - \frac{1}{c_2} + \frac{1}{-\Delta K + c_3} + \frac{1}{\Delta K - c_4} \right. \\
&\left. - \left(\frac{e^{ic_1 W}}{c_1} - \frac{e^{ic_2 W}}{c_2} + \frac{e^{i(-\Delta K + c_3)W}}{-\Delta K + c_3} + \frac{e^{i(\Delta K - c_4)W}}{\Delta K - c_4} \right) \right]
\end{aligned}
\tag{5}
$$

where

$$
\begin{aligned}
c_1 &= k_{n'} - k_n - q \\
c_2 &= k_{n'} - k_n + q \\
c_3 &= k_{n'} + k_n + q \\
c_4 &= k_{n'} + k_n - q
\end{aligned}
\tag{6}
$$

$\Delta K = 4\pi/3a_0$ is the distance between two Dirac points in the $\boldsymbol{k}$-space for 2D graphene band structure, with a_0 = 2.46Å being the lattice constant of graphene. The relaxation time of the nth sub-band is derived as follows:

$$
\begin{aligned}
\frac{1}{\tau_n^{\mp}(E_{\boldsymbol{k}})} &= \sum_{i=1}^{2} \frac{2\pi}{\hbar} \sum_{\boldsymbol{k}',\boldsymbol{q}} \left[n_B^{\mp} |V_{i,\boldsymbol{kk}',\boldsymbol{q}}|^2 \right. \\
&\left. \times \delta(E_{\boldsymbol{k}'} - E_{\boldsymbol{k}} \pm \hbar\omega_{si}) (1 - \cos(\theta_n - \theta_{n'})) \right] \\
&= \sum_{i=1}^{2} \frac{\pi}{\hbar} \frac{A e_0^2 F_i^2}{4W^2} \sum_{q_y} \left[\int_{-\infty}^{\infty} dq_x n_B^{\mp} \frac{e^{-2|\boldsymbol{q}|z}}{|\boldsymbol{q}|} \right. \\
&\left. |T_{n'n}|^2 \left| \frac{E_k \pm \hbar\omega_{si}}{\hbar^2 v_f^2 (k_y + q_y)} \right| (1 - \cos^2(\theta_n - \theta_{n'})) \right]
\end{aligned}
\tag{7}
$$

where $E_{\boldsymbol{k}}$ and $E_{\boldsymbol{k}'}$ are the energy in the initial and final sub-bands, respectively. $n_B^- = 1/[e^{\frac{\hbar\omega_S}{kT}} - 1]$ and $n_B^+ = 1 + n_B^-$ are the phonon number for the absorption and emission processes, respectively. $\hbar\omega_{si}$ is SPP phonon energy. This scattering rate includes contributions from the nth sub-band (intra-band scattering) and neighboring sub-bands (inter-band scattering). Note that the chirality of GNR energy gap is included in the relaxation time calculation.

B. Mobility

Four scattering mechanisms are considered to calculate for total carrier mobility: SPP scattering, Coulomb scattering, AP scattering, and LER scattering. LER scattering plays a significant role for small width GNRs. In the LER scattering calculation, we treat the width as a function of transportation axis. It leads to a modulated band gap and results in the fluctuations in the band-edge potential which induces the scattering of the carriers.

To calculate the mobility for the nth sub-band, the formula $\mu_n=\sigma_n/e_0\rho_{1D}$ is used, where σ_n is the conductance due to the nth sub-band and ρ_{1D} is the total electron density. The $1D$ conductance for the nth sub-band is from [11]

$$\sigma_n = \frac{4e^2}{h}\int_0^\infty \tau_n(E) v_g(E)\left(-\frac{\partial f(E)}{\partial E}\right)dE \qquad (8)$$

where $v_g(E)$ is the electron velocity in the transport direction for the nth sub-band, $f(E)$ is the Fermi-Dirac distribution function, and $\tau_n(E)$ is the relaxation time for the nth sub-band. For SPP scattering, $\tau_n(E)$ is derived from Eq. (7), and for Coulomb scattering, AP scattering, and LER scattering, $\tau_n(E)$ is obtained following [9]. For Coulomb scattering, the surface impurity density is set to 1×10^{11} cm^{-2} with a distance of 1 nm from the surface. Other parameters in the scattering model can be found in [9]. Eight sub-bands are taken into account in the calculation of the carrier mobility arising from a certain scattering mechanism. The zero-point energy is defined in the midpoint of the first conduction band and valence band.

The mobility arising from a certain scattering mechanism is the sum of all the sub-band contributions, which can be obtained from [12]:

$$\mu = \sum_n p_n \mu_n \qquad p_n = \frac{\rho_n}{\rho_{1D}} \qquad (9)$$

where $\rho_{1D} = \sum_n \rho_n$. The nth sub-band electron density is calculated using

$$\rho_n = \int_0^\infty f(E) D_n(E) dE \qquad (10)$$

where

$$D_n(E) = \frac{2}{\pi\hbar v_F}\times\frac{E}{\sqrt{E^2-E_{cn}^2}} \qquad (11)$$

And E_{cn} is the bottom of each sub-band. After determining the carrier mobility from each scattering mechanism, the total carrier mobility can be obtained using Matthiessen's rule

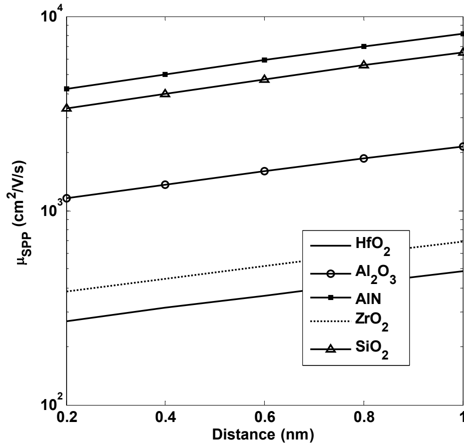

(a)

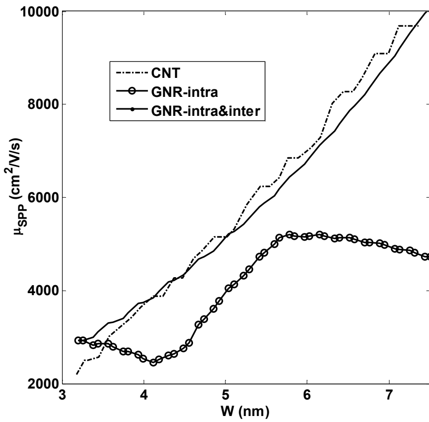

(b)

Figure 2 (a) Carrier mobility due to the SPP scattering mechanism on a 5-nm-wide GNR as a function of the distance between GNR and the surface of the dielectric with Fermi energy level E_F=3/8 E_g. (b) Carrier mobility due to SPP scattering as a function of the GNR (CNT) width (perimeter), where temperature is 300K and E_F=0. The distance between GNR and the surface of the dielectric is 0.4nm.

III. RESULTS

Fig. 2(a) shows that the SPP scattering mobility increases exponentially with the distance between GNR and the surface of the dielectric substrate for different dielectric materials. This tendency can be easily understood in terms of Eq. (2), in which the amplitude of the dielectric polarization of the surface polar phonon decreases exponentially with the distance from the surface of the dielectric substrate. This property suggests a method for weakening the SPP scattering of high-κ dielectric by inserting a thin low-κ dielectric material layer between high-κ dielectric and channel materials consistent with recent experiment [10]. Fig.2 (b) shows the SPP scattering mobility of GNR and CNT for SiO_2 dielectric. The GNR width is taken to be the same as the CNT perimeter. Although the geometry and boundary conditions of GNR and CNT are different, we assume the mobility of the two materials to be similar because of the similarity of the wave function and the band structure. The SPP scattering mobility of CNT is taken from [6]; in which only intra-band scattering is considered. If inter-band scattering is also neglected in the calculation of the SPP scattering mobility for GNR, the two results are quantitatively consistent. When inter-band scattering is added in the calculation, however, the SPP scattering mobility will have a distinct discrepancy. This indicates that the inter-band scattering should not be neglected in calculating for the SPP scattering mobility.

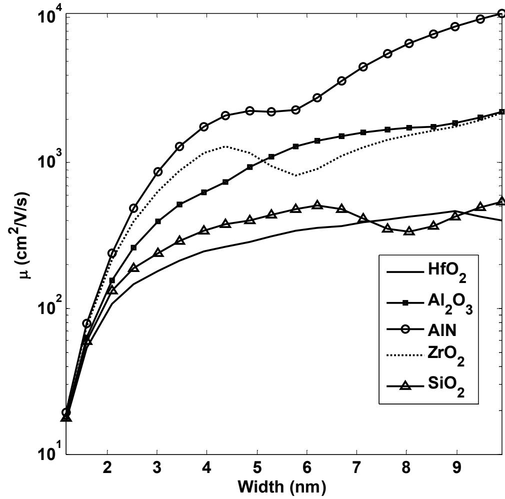

Figure 3 Total Mobility of GNR as a function of GNR width for different dielectrics. Temperature is 300 K and E_F=3/8 E_g. The distance between GNR and the surface of the dielectric is 0.4nm.

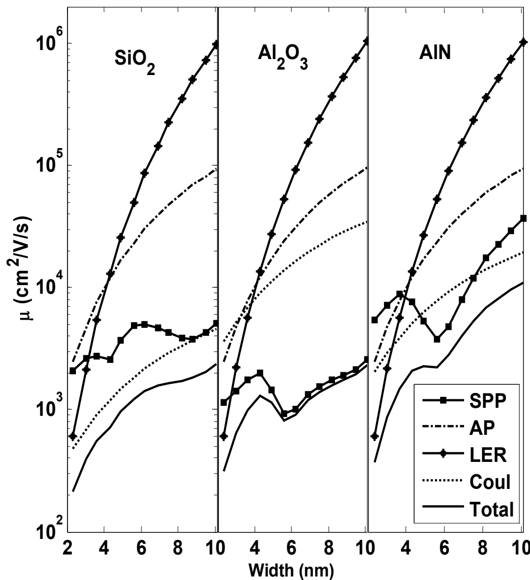

Figure 4 Mobility due to the different scattering mechanisms for GNR with E_F=3/8 E_g as a function of GNR width for SiO_2, Al_2O_3, and AlN. The distance between GNR and the surface of the dielectric is 0.4nm.

Fig. 3 shows the relationship between GNR width and total carrier mobility for different dielectrics. For SiO_2 gate dielectric, the experimental mobilities [2] are less than 100 $cm^2/(V{\cdot}s)$ for a 2 nm-wide GNR and less than 200 $cm^2/(V{\cdot}s)$ for a 3-4 nm-wide GNR. These are consistent with our calculations. To clarify the influence of each scattering mechanism on total carrier mobility for different dielectrics, Fig. 4 shows the carrier mobilities arising from different scattering mechanisms as a function of GNR width for SiO_2, Al_2O_3, and AlN at room temperature. When GNR width is less than 4nm, the LER scattering dominates the total mobility. As the width increases, the surface polar phonon scattering becomes dominant and the LER scattering becomes trivial, especially in Al_2O_3 and AlN. In SiO_2, the mobility is mostly influenced by Coulomb scattering. Since the dielectric constants of Al_2O_3 and AlN are much higher than that of SiO_2, their Coulomb scattering is also much smaller. However, SPP scattering becomes dominant when GNR width is larger than 3 or 4 nm. For AlN, both Coulomb and SPP scattering play important roles in determining total mobility. The SPP scattering of AlN is not as large as in Al_2O_3 because of its strong bond. This is similar to SiO_2. Meanwhile, the Coulomb scattering of AlN is much less than that of SiO_2. Therefore, AlN has the highest mobility at room temperature and may serve as a good gate dielectric.

ACKNOWLEDGMENT

This work is supported by 973 Projects #2011CBA00604 and #2011CB933004, and the National Major Technology Project #2011ZX02707-1.

REFERENCES

[1] K. S. Novoselov, A. K. Geim, S. V. Morozov, D. Jiang, Y. Zhang, S. V. Dubonos, I. V. Grigorieva, and A. A. Firsov, Science **306**, 666 (2004).

[2] X. Wang, Y. Ouyang, X. Li, H. Wang, J. Guo, and H. Dai, Phys. Rev. Lett. **100**, 206803 (2008).

[3] M. V. Fischetti, D. A. Neumayer, and E. Cartier, J. Appl. Phys. **90**, 4587 (2001).

[4] S. Fratini and F. Guinea, Phys. Rev. B **77**,195415 (2008).

[5] A. Konar, T. Fang, and D. Jena, arXiv:0902.0819v1(2009).

[6] V. Perebeinos, S. V. Rotkin, A. G. Petrov, and P. Avourist, Nano Lett. **9**, 1 (2009).

[7] G. D. Mahan, Phys. Rev. B **5**, 739 (1972).

[8] L. Brey and H. A. Fertig, Phys. Rev. B **73**, 235411 (2006).

[9] T. Fang, A. Konar, H. Xing, and D. Jena, Phys. Rev. B **78**, 205403 (2008).

[10] D. B. Farmer, H.-Y. Chiu, Y.-M. Lin, K. A. Jenkins, F. Xia, and P. Avouris, Nano Lett. **9**, 12 (2009).

[11] K. Seeger, Semiconductor Physics: An Introduction, Springer-Verlag Berlin Heidelberg New York, pp 49-51 (1982).

[12] S. Dhar, H. Kosina, V. Palankovs.ki, S. E. Ungersbock, and S. Selberherr, IEEE Transactions on Electron Devices **52**, 4 (2005).